

# Same-sign $W$ pair production as a probe of double parton scattering at the LHC

Jonathan R. Gaunt<sup>1</sup>, Chun-Hay Kom<sup>1</sup>, Anna Kulesza<sup>2</sup>, and W. James Stirling<sup>1</sup>

<sup>1</sup> Cavendish Laboratory, J.J. Thomson Avenue, Cambridge CB3 0HE, UK

<sup>2</sup> Institute for Theoretical Particle Physics and Cosmology, RWTH Aachen University D-52056 Aachen, Germany

November 6, 2018

**Abstract.** We study the production of same-sign  $W$  boson pairs at the LHC in double parton interactions. Compared with simple factorised double parton distributions (dPDFs), we show that the recently developed dPDFs, GS09, lead to non-trivial kinematic correlations between the  $W$  bosons. A numerical study of the prospects for observing this process using same-sign dilepton signatures, including  $W^\pm W^\pm jj$ , di-boson and heavy flavour backgrounds, at 14 TeV centre-of-mass energy is then performed. It is shown that a small excess of same-sign dilepton events from double parton scattering over a background dominated by single scattering  $W^\pm Z(\gamma^*)$  production could be observed at the LHC.

## 1 Introduction

The Large Hadron Collider (LHC) at CERN will offer many interesting tests of Standard Model (SM) physics and, indeed, a precise knowledge of SM processes is necessary to identify unambiguously New Physics (NP) signals from SM backgrounds. The high LHC collision energy will open up a new kinematic regime in which certain SM processes will become precisely measureable for the first time. An example is multiple parton hard-scattering, i.e. events in which two or more distinct hard parton interactions occur simultaneously. The theoretical study of such processes goes back to the early days of the parton model [1–3] with subsequent extension to perturbative QCD [4–16]. Experimental evidence for double parton scattering (DPS) has been found in  $\sqrt{s} = 63$  GeV  $pp$  collisions by the AFS collaboration at the CERN ISR [17], and more recently in  $\sqrt{s} = 1.8$  TeV  $p\bar{p}$  collisions by the CDF collaboration [18] and  $\sqrt{s} = 1.96$  TeV  $p\bar{p}$  collisions by the D0 collaboration [19] at the Fermilab Tevatron.

In the standard framework for calculating inclusive hard-scattering cross sections in hadron-hadron collisions, it is assumed that only one hard interaction occurs per collision (plus multiple soft interactions). This assumption is typically justified on the grounds that the probability of a hard parton-parton interaction in a collision is very small. Thus the probability of having two or more hard interactions in a collision is highly suppressed with respect to the single interaction probability.

However, as the collider centre-of-mass energy becomes larger, we may expect multiple hard parton collisions to become more important. This can be understood as follows. Consider a final state consisting of the products of two hard collisions  $A$  and  $B$ , where for example  $A, B =$

$W, Z, jj, t\bar{t}, \dots$  etc. It is commonly assumed that double parton scattering cross sections  $\sigma_{(A,B)}^{DPS}$  can be approximately factorised into the product of two single scattering cross sections:

$$\sigma_{(A,B)}^{DPS} = \frac{m}{2} \frac{\sigma_{(A)}^S \sigma_{(B)}^S}{\sigma_{\text{eff}}} \quad (1)$$

where the quantity  $m$  is a symmetry factor that equals 1 if  $A = B$  and 2 otherwise. The factor  $\sigma_{\text{eff}}$  in the denominator has the dimensions of a cross section. The reason for this is that given that one hard scattering occurs, the probability of the other hard scattering is proportional to the flux of accompanying partons; these are confined to the colliding protons, and therefore their flux should be inversely proportional to the area (cross section) of a proton. Of course the  $(A, B)$  final state can also be produced by a single parton scattering, with cross section  $\sigma_{(AB)}^S$ . If the masses of the final states  $A$  and  $B$  are fixed, then the collider energy ( $\sqrt{s}$ ) dependence of the hadronic cross sections is controlled by the  $x$  dependence of the parton distribution functions (PDFs). Because the PDFs increase rapidly with  $x$  as  $x \rightarrow 0$ , the cross sections increase with  $\sqrt{s}$ . This implies that  $\sigma_{(A,B)}^D$ , which is proportional to a product of single scattering cross sections, will increase more rapidly with  $\sqrt{s}$  than  $\sigma_{(AB)}^S$ . This raises the possibility that multiple hard parton scattering, which has received relatively little attention to date, could provide important backgrounds to NP signals at the LHC [20–23]. To take a simple example for SM Higgs production, the ‘standard’ irreducible background to associated  $Z + H(\rightarrow b\bar{b})$  production is  $q\bar{q}, gg \rightarrow Zb\bar{b}$ . However, there is an additional DPS background with  $A = Z$  and  $B = b\bar{b}$ .

Of course the magnitude of the DPS cross section is directly dependent on the size of  $\sigma_{\text{eff}}$  in Eq. (1). The recent CDF and D0 measurements [18, 19] at the Tevatron, utilising the  $\gamma + 3\text{jet}$  final state with  $A$  corresponding to  $\gamma + \text{jet}$  production and  $B$  to dijet production, suggest  $\sigma_{\text{eff}} \sim 15$  mb, which is roughly 20% of the total (elastic + inelastic)  $p\bar{p}$  cross section at the Tevatron collider energy. The non-perturbative physics that determines  $\sigma_{\text{eff}}$  is not well enough understood to be able to predict its value at the LHC. If it is proportional to the total inelastic cross section, one might expect a slightly higher value at LHC energies. Given this uncertainty, the best approach is clearly to find a *benchmark* double scattering process for the LHC, from which  $\sigma_{\text{eff}}$  can be determined. This will not only serve to calibrate DPS backgrounds to NP processes, but will also provide important information on the non-perturbative structure of the proton.

In fact, Eq. (1) is only an approximation to the following more general expression:

$$\begin{aligned} \sigma_{(A,B)}^{DPS} = & \frac{m}{2} \sum_{i,j,k,l} \int dx_1 dx_2 dx'_1 dx'_2 d^2b \\ & \times \Gamma_{ij}(x_1, x_2, b; t_1, t_2) \Gamma_{kl}(x'_1, x'_2, b; t_1, t_2) \\ & \times \hat{\sigma}_{ik}^A(x_1, x'_1) \hat{\sigma}_{jl}^B(x_2, x'_2). \end{aligned} \quad (2)$$

The  $\Gamma_{ij}(x_1, x_2, b; t_1, t_2)$  represent generalised double parton distributions. They may be loosely interpreted as the inclusive probability distributions to find a parton  $i$  with longitudinal momentum fraction  $x_1$  at scale  $t_1 \equiv \ln(Q_1^2)$  in the proton, in addition to a parton  $j$  with longitudinal momentum fraction  $x_2$  at scale  $t_2 \equiv \ln(Q_2^2)$ , with the two partons separated by a transverse distance  $b$ . The scale  $t_1$  is given by the characteristic scale of subprocess  $A$ , whilst  $t_2$  is equal to the characteristic scale of subprocess  $B$ .

It is typically taken that  $\Gamma_{ij}(x_1, x_2, b; t_1, t_2)$  may be decomposed in terms of longitudinal and transverse components as follows:

$$\Gamma_{ij}(x_1, x_2, b; t_1, t_2) = D_h^{ij}(x_1, x_2; t_1, t_2) F_j^i(b). \quad (3)$$

Making the further assumption that  $F_j^i(b)$  is the same for all parton pairs  $ij$  involved in the DPS of interest, this leads to:

$$\begin{aligned} \sigma_{(A,B)}^{DPS} = & \frac{m}{2\sigma_{\text{eff}}} \sum_{i,j,k,l} \int dx_1 dx_2 dx'_1 dx'_2 \\ & \times D_p^{ij}(x_1, x_2; t_1, t_2) D_p^{kl}(x'_1, x'_2; t_1, t_2) \\ & \times \hat{\sigma}_{ik}^A(x_1, x'_1) \hat{\sigma}_{jl}^B(x_2, x'_2), \\ \sigma_{\text{eff}} = & \left[ \int d^2b (F(b))^2 \right]^{-1}. \end{aligned} \quad (4)$$

If one ignores longitudinal momentum correlations such that the components  $D_h^{ij}$  take the form  $D_h^{ij}(x_1, x_2; t_1, t_2) = D_h^i(x_1; t_1) D_h^j(x_2; t_2)$ , then one finally arrives at the form of Eq. (1). This is the approach that has been taken in existing phenomenological calculations regarding DPS [20–27]. Such an approximation is typically justified at low  $x$

values on the grounds that the population of partons is large at these values.

On the other hand, a number of theoretical studies [28–31] have suggested that non-negligible longitudinal momentum correlations do exist in the double parton distributions (dPDFs)  $D_h^{ij}(x_1, x_2; t_1, t_2)$ . These papers have investigated the special case in which the two factorisation scale arguments of the dPDFs are set equal  $t_1 = t_2 = t$ . In [28, 30, 31], it is shown that pQCD (‘double DGLAP’) evolution causes the dPDFs to deviate from factorised forms, such that even if factorised forms are a good approximation at low scales, they cannot be so at higher scales. Ref. [29] goes further, and shows that as a result of the sum rules the dPDFs have to obey, the PDF factorisation hypothesis  $D^{ij} = D^i D^j$  cannot hold for any  $i, j$  at any scale  $t$  – although it may be a reasonable approximation for sea quark and gluon distributions at small  $x$ .

Thus, a more accurate way to model DPS is to use Eq. (4) along with a set of dPDFs which incorporates the effects of pQCD evolution and sum rule constraints (e.g. GS09 [29]). The practical implication of the longitudinal momentum correlations inherent in the GS09 set is that the final states  $A$  and  $B$  will necessarily be correlated in longitudinal momentum, and in particular the rapidity distribution of  $A$  will not be independent of that of  $B$ .

In this study we focus on same-sign  $W$  pair production at the LHC as the paradigm DPS benchmark process, i.e.  $A = B = W^+$  and  $A = B = W^-$ . In this context,  $W^\pm W^\pm$  production was first discussed in Ref. [24] and subsequently studied in more detail in Ref. [31] and Refs. [25, 26], the latter of which also compared the cross sections of DPS  $W^\pm W^\pm$  and  $W^\pm W^\pm jj$  in single scattering with the inclusion of kinematic cuts. We will investigate not only the magnitude of the DPS cross sections, but also the rapidity correlations for the DPS  $W^\pm W^\pm$  final state, both for the GS09 dPDFs and for a simple factorised PDF model. Note that the recent CDF and D0 measurements are not accurate enough to distinguish these: the CDF result [18] in particular shows no sign of  $x$ -dependence in the  $\sigma_{\text{eff}}$  measured.

In assessing suitable benchmark processes for DPS at LHC, one should of course choose a signal channel for which the single scattering background is suppressed. We will be interested in  $W^\pm W^\pm$  final states in which both  $W$  bosons decay leptonically,  $W \rightarrow l\nu$  with  $l = e, \mu$ . This results in same-sign dilepton (SSL) signals which we will investigate in detail.  $W^\pm W^\pm$  production has the advantage that same-sign single scattering is forbidden at the same order in the SM, i.e. there is no  $ij \rightarrow W^+ W^+, W^- W^-$  contribution (cf.  $q\bar{q} \rightarrow W^+ W^-, ZZ$ ). The lowest order ‘background’ process is  $W^\pm W^\pm jj$ , which is of order  $\mathcal{O}(\alpha^4)$  or  $\mathcal{O}(\alpha_S^2 \alpha^2)$ . As we shall see, the presence of extra jets serves as an efficient tag to veto this background. The possibility of using lepton pseudorapidity distribution to enhance the DPS signal was considered in [32, 33]. For these reasons, it was believed that the same-sign dilepton channel provides a ‘clean environment’ for studying DPS processes. However there are other important backgrounds, for example  $W^\pm Z(\gamma^*)$  and  $b\bar{b}$  production, both

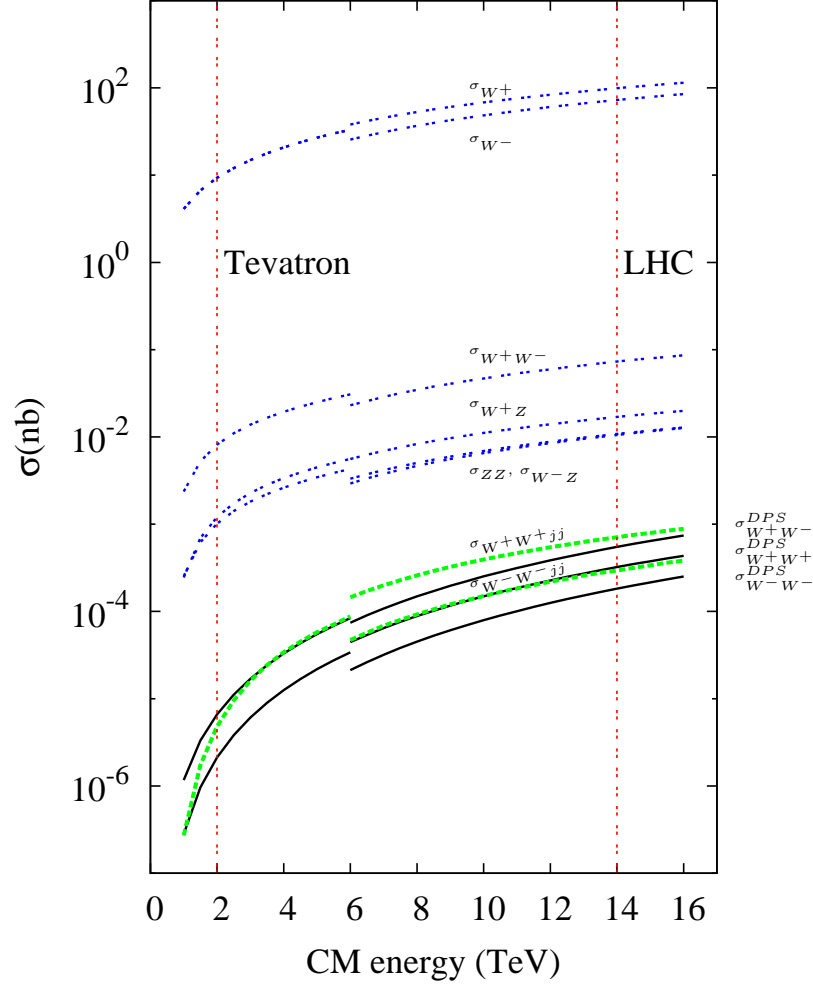


**Fig. 1.** Cross sections of various processes in proton (anti-)proton collisions as a function of  $\sqrt{s}$ . The dotted curves correspond to single scattering processes, while the solid curves correspond to double scattering processes computed using GS09 dPDFs. From top down, the  $p\bar{p}$  single scattering cross sections in the Tevatron region are  $\sigma_{W^\pm}$ ,  $\sigma_{W^+W^-}$ ,  $\sigma_{W^\pm Z}$ ,  $\sigma_{ZZ}$  and  $\sigma_{W^\pm W^\pm jj}$ . The double scattering cross sections are  $\sigma_{W^+W^-}^{DPS}$  and  $\sigma_{W^\pm W^\pm}^{DPS}$ . In the LHC region, the dotted curves are  $pp$  cross sections of  $\sigma_{W^+}$ ,  $\sigma_{W^-}$ ,  $\sigma_{W^+W^-}$ ,  $\sigma_{W^\pm Z}$ ,  $\sigma_{ZZ}$ ,  $\sigma_{W^-Z}$ ,  $\sigma_{W^+W^+jj}$  and  $\sigma_{W^-W^-jj}$ , while the solid curves are  $\sigma_{W^+W^-}^{DPS}$ ,  $\sigma_{W^+W^+}^{DPS}$  and  $\sigma_{W^-W^-}^{DPS}$ .

of which can produce a pair of same-sign leptons and missing  $E_T$ . The former leads to a SSL signal when the ‘wrong’ sign lepton from  $Z$  decay falls outside the detector acceptance, whereas for the latter, SSL events result when a neutral  $B^0$  meson undergoes  $B^0$ - $\bar{B}^0$  mixing, followed by leptonic decays. These backgrounds have not been studied in detail in the context of di-boson production (a brief discussion of the  $W^\pm Z(\gamma^*)$  background can be found in [34]). We will go beyond comparing the DPS  $W^\pm W^\pm$  signal and SPS  $W^\pm W^\pm jj$  background [24–26] to explore the impact of a fairly standard choice of lepton cuts on SSL events from both the signal and backgrounds.

This paper is organised as follows. In the following section we discuss in detail the calculation of the signal  $W^\pm W^\pm \rightarrow l^\pm l^\pm \nu\nu$  DPS process cross section. We compare total cross sections and rapidity distributions

obtained using GS09 dPDFs and approximate factorised dPDFs. In Sections 3 and 4 we study a number of important background contributions to the SSL signal, and investigate to what extent they can be suppressed through final-state cuts. Our conclusions on the observability of DPS at the LHC in the  $WW$  SSL channel are presented in Section 5.

## 2 Signal processes: leptonic channels of $W^\pm W^\pm$

The DPS signal consists of two same-sign leptons and missing energy, coming from the decay of two same-sign  $W$  bosons. The leptons are produced in two simultaneous

partonic processes

$$ij \rightarrow W^\pm + X \rightarrow l^\pm + \nu_l + X. \quad (5)$$

The predictions for the DPS signal are calculated according to Eq. (4). Total cross sections and distributions are obtained for four sets of dPDFs: GS09 from [29], and factorized dPDFs of the form<sup>1</sup>

$$D_h^{ab}(x_1, x_2, t) = D_h^a(x_1, t) D_h^b(x_2, t) \theta(1 - x_1 - x_2) \times (1 - x_1 - x_2)^n \quad n = 0, 1, 2, \quad (6)$$

hereafter referred to as MSTW<sub>*n*</sub> sets. The sPDFs  $D_h^i(x, t)$  are taken from the MSTW 2008 LO set. As pointed out in [29], these factorised sets do not satisfy dDGLAP evolution or consistent sets of sum rules, although with an appropriately chosen value of  $n$  they can provide a reasonable approximation to the ‘exact’ GS09 dPDFs. The factorization scale in the calculations of the DPS signal is fixed at  $\mu_F = M_W$  for all parton sets.

The partonic cross sections in Eq. (4) are calculated at leading order. At this level, the transverse momentum ( $p_T$ ) distribution of the produced  $W$  bosons is zero. When we come to consider signals and backgrounds with realistic experimental cuts, we will need to provide realistic descriptions of kinematic distributions, in particular of transverse quantities like the leptonic  $p_T$  and  $\cancel{E}_T$ , see Section 4.

All numerical results are evaluated with the following electroweak input parameters [36]:  $M_Z = 91.188$  GeV,  $M_W = 80.398$  GeV,  $G_F = 0.116637 \times 10^{-5}$  GeV<sup>-2</sup>,  $\Gamma_Z = 2.50$  GeV and  $\Gamma_W = 2.14$  GeV. Other EW couplings are derived using tree level relations. The effective branching ratio  $\mathcal{BR}(W^+ \rightarrow \mu^+ \nu_\mu)$ , using  $\Gamma_W$  as the total width, is 0.106. The CKM mixing parameters used are  $|V_{us}| = 0.226$ ,  $|V_{ub}| = 0.004$ ,  $|V_{cd}| = 0.230$ ,  $|V_{cb}| = 0.041$ , and other parameters are obtained using unitarity constraints. We take the value of  $\sigma_{\text{eff}} = 14.5$  mb, consistent with the Tevatron measurements.

A comparison of the cross sections for DPS and SPS  $WW$  production processes as a function of collider centre-of-mass (CM) energy  $\sqrt{s}$  is shown in Fig. 1. The DPS cross sections are obtained with the GS09 set of dPDFs. We see immediately that while the single scattering  $q\bar{q} \rightarrow W^+W^-, W^\pm Z, ZZ$  cross sections dominate at all collider energies, the DPS  $W^\pm W^\pm$  and SPS  $W^\pm W^\pm jj$  cross sections are comparable in magnitude. As we shall demonstrate, with an appropriate set of jet veto cuts the SPS  $W^\pm W^\pm jj$  cross sections can be significantly reduced. We quote the values of the total cross section for DPS  $WW$  production processes for various CM energies at the LHC in Table 1. In Tables 1 and 2 we show also the values of the ratio

$$R \equiv 4 \frac{\sigma_{W^+W^+} \sigma_{W^-W^-}}{\sigma_{W^+W^-}^2}$$

which measures the deviation from the factorisation approach, Eq. (1). When  $R = 1$ , factorisation is exact. We note that factorisation is broken at the 20% to 30% level, and the approximation improves at the higher collider energies as lower  $x$  regions are probed.

	$\sigma_{\text{GS09}}$		
	$\sqrt{s} = 7$ TeV	$\sqrt{s} = 10$ TeV	$\sqrt{s} = 14$ TeV
$W^+W^-$	0.107	0.250	0.546
$W^+W^+$	0.0640	0.148	0.321
$W^-W^-$	0.0317	0.0793	0.182
$R$			
	0.709	0.751	0.784

**Table 1.** DPS  $WW$  total cross sections (in pb) for  $pp$  collisions at different CM energies. The values are obtained by first calculating the leptonic cross sections, before dividing by the corresponding branching ratios. All cross sections are evaluated using GS09 parton distributions. The ratio  $R$  measures deviation from the factorisation approach, as explained in the text.

	$\sigma_{\text{GS09}}$	$\sigma_{\text{MSTW}_0}$	$\sigma_{\text{MSTW}_1}$	$\sigma_{\text{MSTW}_2}$
$W^+W^-$	0.546	0.496	0.409	0.348
$W^+W^+$	0.321	0.338	0.269	0.223
$W^-W^-$	0.182	0.182	0.156	0.136
$R$				
	0.784	1.00	1.00	1.00

**Table 2.** DPS  $WW$  total cross sections (in pb) for  $pp$  collisions at  $\sqrt{s} = 14$  TeV evaluated using different dPDFs sets. The values are obtained by first calculating the leptonic cross sections, before dividing by the corresponding branching ratios.

Since the DPS total cross sections are most relevant for the LHC with  $\sqrt{s} = 14$  TeV, we will focus our analysis on this case. It is interesting to investigate the effect of the different sets of the dPDFs, *cf.* Table 2. Note that all the factorised distributions contain a kinematic factor  $\theta(1 - x_1 - x_2)$ , which automatically implies  $R \neq 1$  for these sets, although the effect is numerically very small at LHC (14 TeV) energies where small  $x$  values are probed. The DPS total cross sections for same-sign  $W^\pm W^\pm$  production are very similar when using the GS09 and MSTW<sub>0</sub> sets whereas the values for the MSTW<sub>1</sub> and MSTW<sub>2</sub> sets are smaller due to the suppression caused by the  $(1 - x_1 - x_2)^n$  factors. The DPS opposite-sign  $W^\pm W^\mp$  cross section is somewhat larger for GS09 than for MSTW<sub>0</sub>. This is because of an enhancement of the  $D^{q\bar{q}}$  ( $q = u, d$ ) GS09 dPDFs induced by the  $g \rightarrow q\bar{q}$  contribution to dDGLAP evolution [29]. We also observe that the MSTW<sub>0</sub>  $W^+W^+$  cross section is slightly larger than its GS09 counterpart, whereas such a difference is not observed in the  $W^-W^-$  cross sections. The probable explanation behind this is the following. Both the  $uu$  and  $dd$  inputs to GS09 consist of (roughly) factorised forms minus terms to take account of number effects ( $\frac{1}{2}D^{u\nu}D^{u\nu}$  and  $D^{d\nu}D^{d\nu}$  respectively). In absolute terms, the subtraction from the  $uu$  input is larger than that from the  $dd$  (since  $\frac{1}{2}D^{u\nu}D^{u\nu} \approx 2D^{d\nu}D^{d\nu}$ ). This results in a greater decrease of the GS09  $W^+W^+$  cross section relative to that of MSTW<sub>0</sub> than occurs for  $W^-W^-$  production. In fact, the  $W^-W^-$  cross section for GS09 ends up being roughly equal to that of MSTW<sub>0</sub>, since all GS09 dPDFs are ‘fed’ by the sPDFs during evolution (ei-

<sup>1</sup> We use the notation  $t = \ln \mu_F^2$ .

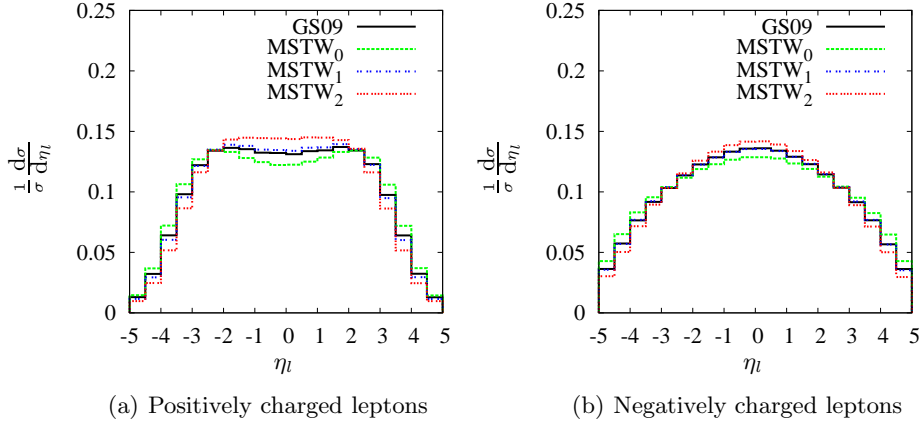


**Fig. 2.** Normalised lepton pseudorapidity distributions for  $pp$  collisions at  $\sqrt{s} = 14$  TeV evaluated using different dPDFs. No cuts are applied.

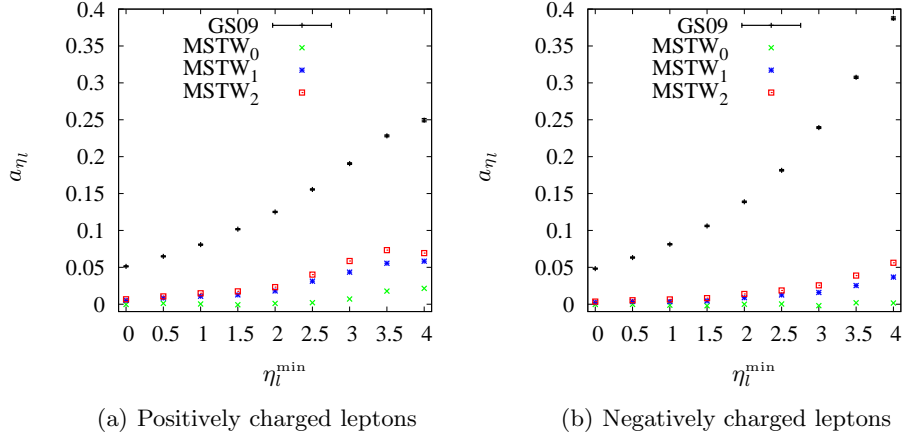


**Fig. 3.** Pseudorapidity asymmetry  $a_{\eta_l}$  for  $pp$  collisions at  $\sqrt{s} = 14$  TeV evaluated using different dPDFs. No cuts are applied.

ther directly or indirectly via the  $gg$  dPDF). The ‘sPDF feed’ contribution to the GS09 dPDFs compensates for the subtraction from the  $dd$  input in the case of the  $W^-W^-$  cross section. On the other hand, a similar sPDF feed contribution cannot counterbalance the greater subtraction from the  $uu$  input in the  $W^+W^+$  case, causing the GS09  $W^+W^+$  cross section to be smaller than the MSTW<sub>0</sub> cross section. Obviously, the deviations from the factorization approach measured by the ratio  $R$  are small when using the MSTW <sub>$n$</sub>  sets. In GS09, there are sizeable deviations from factorisation, particularly in the valence sector (i.e.  $D^{q\nu q\nu} \neq D^{q\nu} D^{q\nu}$ ), and these are reflected in smaller values of  $R$ .

In order to study the potential of using same-sign  $WW$  production for measuring DPS, a full study of the signal, including leptonic decays and cuts, is necessary. In Fig. 2(a) we present the normalised pseudorapidity distribution of the  $l^+$  leptons,  $\frac{1}{\sigma} \frac{d\sigma}{d\eta_l}$ , for different sets of dPDFs.

Although visible, the differences in the lepton pseudorapidity distributions for the various dPDFs are small. The effect of the correlations in the longitudinal momentum fractions in the GS09 set is closely reproduced by the MSTW<sub>1</sub> set, a result which could be expected from the comparative study of GS09 and MSTW <sub>$n$</sub>  distributions in [29]. Fig. 2(b) shows the corresponding plot for  $l^-$  leptons. Although the shapes of the pseudorapidity distributions are different (a simple reflection of the difference between  $u$  and  $d$  quark PDFs), the qualitative differences between the various sets for  $l^-$  are the same as for  $l^+$  production.

The sensitivity to longitudinal correlations can be maximized in the following asymmetry

$$a_{\eta_l} = \frac{\sigma(\eta_{l_1} \times \eta_{l_2} < 0) - \sigma(\eta_{l_1} \times \eta_{l_2} > 0)}{\sigma(\eta_{l_1} \times \eta_{l_2} < 0) + \sigma(\eta_{l_1} \times \eta_{l_2} > 0)}, \quad (7)$$

where  $\eta_l$  is the lepton pseudorapidity, and  $|\eta_{l_1}|, |\eta_{l_2}| > \eta_l^{\min}$ . The asymmetry measures the extent to which the presence of one  $W$  produced at high rapidity affects the probability of finding another  $W$  boson with similarly large rapidity. A positive  $a_{\eta_l}$  means that the leptons prefer to lie in opposite hemisphere. For higher values of  $\eta_l^{\min}$  the effect of the correlations becomes more pronounced, *cf.* Figs. 3(a) and 3(b). Such behaviour is to be expected as the correlations are most important for the distributions probed at high values of  $x$  for both partons in the same proton, reached when the leptons ( $W$  bosons) are produced at high rapidities.

In this section we have restricted our attention to basic quantities (total cross sections and pseudorapidity distributions) to illustrate the impact of the various dPDF sets, and in particular the effect of the correlations that are a feature of the GS09 set. As we shall see below, in practice we have to introduce further cuts on the final-state particles in order to suppress large backgrounds from SPS processes. In Section 4 we will investigate the effects on DPS event rates and correlations after imposing these cuts.

### 3 Backgrounds

We now turn to discuss background contributions. Recall that a signal event consists of two same-sign charged leptons plus missing transverse energy, where the leptons originate in two separate hard scatterings from one  $pp$  collision. As already mentioned,  $W^\pm W^\pm jj$  single scattering provides the lowest order, irreducible background. Heavy flavour production and gauge boson pair production can also lead to same-sign dilepton events. We shall discuss the relevant properties of these background contributions, and propose cuts that can reduce them.

#### 3.1 The $W^\pm W^\pm jj$ single scattering background

In single scattering, the lowest order in which same-sign  $W$ 's can be produced are  $\mathcal{O}(\alpha_S^2 \alpha^2)$  and  $\mathcal{O}(\alpha^4)$ . By considering overall charge conservation, one sees that all the participating partons must be quarks. The QCD diagrams involve two quark propagators and exchange of a  $t$ -channel gluon, whereas neutral electroweak gauge boson and Higgs exchanges are also possible for the EW contributions. As shown in Fig. 1, the cross sections for  $W^\pm W^\pm jj$  and the DPS  $W^\pm W^\pm$  signal are of the same order of magnitude at LHC energies.

The presence of jets provide an important handle to suppress this single scattering background. The presence of two  $W$ 's implies that the jet energies are typically of the order of the weak scale,  $M_W$ , and their  $p_T$  distribution can have a long tail. A veto of events with (central) high  $p_T$  jets will therefore be useful in suppressing this background. In Fig. 4, we show the variation of the cross section of  $\sigma(pp \rightarrow W^+ W^+ jj) \cdot [\mathcal{BR}(W^+ \rightarrow \mu^+ \nu_\mu)]^2$  with maximum transverse momentum ( $\max p_{Tj}$ ) and minimum pseudorapidity ( $\eta_j^{\min}$ ) of the jets allowed in an event. For

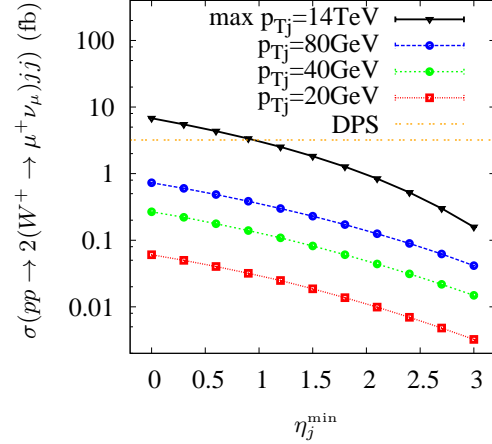


**Fig. 4.**  $\sigma(pp \rightarrow W^+ W^+ jj) \cdot [\mathcal{BR}(W^+ \rightarrow \mu^+ \nu_\mu)]^2$  (fb) as a function of  $\max p_{Tj}$  and  $\eta_j^{\min}$ . No other cuts are applied.

example, we see that vetoing events with jet  $p_T > 20$  GeV with no pseudorapidity requirement suppresses the cross section to about two orders of magnitude below the signal (DPS) cross section. We conclude that this background can be effectively suppressed by a jet veto, and so will not be discussed further. However we note in passing that this process may contribute to SSL backgrounds in beyond SM scenarios, particularly in event topologies including jets, for example single slepton production in supersymmetry without R-parity.

#### 3.2 The heavy flavour background

The heavy flavour production processes  $pp \rightarrow Q\bar{Q} + X$  with  $Q = t, b$  can lead to SSL events. In  $t\bar{t}$  production, the dominant contribution to same-sign dilepton events is where both a top and the bottom of the other top decay semi-leptonically, for example

$$\begin{aligned} t &\rightarrow W^+ b \rightarrow l^+ \nu b, \\ \bar{t} &\rightarrow W^- \bar{b} \rightarrow q\bar{q}' l^+ \nu c. \end{aligned} \quad (8)$$

The final state is therefore nominally  $l^+ l^+ + 2\nu + 4$  jets. Requiring two leptons of the same-sign means that one of the leptons should come from  $b$ -quark decay. This is important because the  $b$ -quark, originating from top decay, is energetic and its daughter lepton will generally not be isolated from the other (hadronic) decay products. Hence a tight lepton isolation requirement will be effective in reducing this background. The lepton from the  $W$  typically acquires a harder  $p_T$  spectrum than the signal leptons. Imposing a maximum lepton  $p_T$  cut will therefore also be useful. Similarly to the  $W^\pm W^\pm jj$  process, the presence of energetic jets again provides an effective suppression mechanism. Because of these considerations, we expect that  $t\bar{t}$  production will only contribute subdominantly to

the background, and therefore will also be neglected in our numerical analysis.

In  $b\bar{b}$  production, the hard process is initiated by two gluons. To obtain same-sign dileptons, the two resulting  $B$  mesons should decay semi-leptonically. Further, one of the  $B$  mesons must undergo  $B^0$ - $\bar{B}^0$  mixing before decay, which is possible if the  $B$  meson is neutral. The relevant processes are thus:

$$\begin{aligned} gg &\rightarrow b\bar{b} \rightarrow B\bar{B} + \dots, \\ B &\rightarrow l^+ \nu X, \\ \bar{B}^0 &\rightarrow B^0 \rightarrow l^+ \nu \tilde{X}, \end{aligned} \quad (9)$$

together with the charge conjugation processes.

Due to its large production cross section at the LHC, this can be a problematic background (a detailed study of heavy flavour backgrounds to lepton-pair-plus-missing-transverse-energy final states can be found, for example, in Ref. [35]). Fortunately, the kinematic properties of this process are very different from those of the signal, as the two scales involved are very different ( $m_b$  vs.  $M_W$ ). For example, the lepton  $p_T$  from  $b\bar{b}$  decay peaks at very low values and decreases exponentially as  $p_T$  increases. As the  $p_T$  of the leptons comes primarily from the  $p_T$  of the parent  $B$  mesons, at high  $p_T$  the lepton will tend to align with other hadronic decay products making isolation difficult. An energetic isolated lepton will also tend to be accompanied by a soft neutrino, leading to low transverse missing energy  $\cancel{E}_T$ . As a result, a combination of lepton isolation, minimum  $p_T$  and  $\cancel{E}_T$  cuts should effectively suppress this background. We shall study the impact of these cuts in the numerical simulation in the following section.

The  $c\bar{c}$  process also leads to same-sign dilepton events through a mechanism similar to that of  $b\bar{b}$ . In this case, the lepton  $p_T$  spectra peaks at even lower values. As well as having a strongly suppressed contribution in our  $p_T$  region of interest, the leptons are again difficult to be isolated from the other decay products, and low  $\cancel{E}_T$  is expected. As a result, the lepton cuts used to suppress the  $b\bar{b}$  background should effectively suppress  $c\bar{c}$  events as well.

### 3.3 The electroweak gauge boson pair background

In principle, the production and leptonic decay of heavy weak boson pairs,  $VV \rightarrow 4$  leptons with  $V = W, Z$  can also provide a sizeable background. However these processes do not naturally give rise to events with same-sign lepton pairs as the only visible particles. For example,  $W^\pm Z(\gamma^*)$  and  $Z(\gamma^*)Z(\gamma^*)$  can lead to 3 or 4 charged leptons respectively, and can mimic the same-sign di-lepton signal if the ‘wrong’ sign leptons are not detected. This happens if they fall outside the detector acceptance, or if they are not reconstructed. The relevant processes are then

$$\begin{aligned} q\bar{q}' &\rightarrow W^+ Z(\gamma^*) \rightarrow l^+ \nu l^+ (l^-), \\ q\bar{q} &\rightarrow Z(\gamma^*) Z(\gamma^*) \rightarrow l^+ (l^-) l^+ (l^-), \end{aligned} \quad (10)$$

and their charge-conjugated processes. In the above expressions the leptons in brackets are not identified. Clearly,

a wrong sign lepton veto will be able to reduce this background when more than 2 leptons are identified. The virtual  $\gamma^*$  can still contribute significantly when it decays asymmetrically into a hard and a soft lepton in the central region. Following [37], this may be suppressed by looking for isolated charged tracks that form a low invariant mass with one of the same-sign leptons. For the  $Z$ , the dominant contribution is when the wrong sign lepton lies outside the central region and is not reconstructed as a lepton. This in turn pulls its partner lepton towards the large pseudorapidity region, potentially providing a shape variable for further discrimination. Furthermore, the lepton  $p_T$  spectrum extends beyond that of the DPS signal, and therefore a maximum lepton  $p_T$  cut will be useful.

### 3.4 Other backgrounds

Another possible source of same-sign lepton pairs comes from multi-particle interactions, when production of  $W$ ’s of the same sign from two separate proton collisions occurs during the same bunch crossing. In the factorised dPDF approximation, this background and the signal, where the double scattering occurs in one proton-proton collision, are expected to exhibit similar kinematic properties. However the leptons from the multi-particle-interaction background will in general have tracks pointing back to two different locations along the beam axis. In the Appendix, we perform a simple estimation to show that reasonable longitudinal vertex resolution in the LHC detectors should allow significant suppression of these events.

Apart from the physics backgrounds discussed, non-physics backgrounds can also be important. For example,  $W$ +jets may contribute when a jet is mis-identified as a lepton, or  $ZZ$  production may contribute when one  $Z$  decays invisibly and the charge of a lepton from the decay of the other  $Z$  is mis-identified. A thorough investigation of these effects requires a detailed detector simulation. This is beyond the scope of the present study, and so we restrict ourselves to studying the effect of physics backgrounds only.

## 4 Numerical Study

In the previous two sections we have discussed the DPS signal, and its characteristic properties, and the most important single scattering backgrounds. In this section we carry out numerical studies to investigate the relative size of the various contributions and how to reduce them.

We first discuss the cuts, referred to as ‘basic cuts’ below, applied in our numerical analysis. They are ‘basic’ in the sense that they are necessary to reduce the background to a manageable level, while keeping the signal largely intact. Later we shall discuss refinements that can improve the signal to background ratio, but at a price of further reducing the signal.

As discussed in the previous section, the  $W^\pm W^\pm jj$  and  $t\bar{t}$  will (the latter partly) be suppressed by a jet veto. In particular, rejecting events with jets having  $p_T > 20$

GeV will suppress the  $W^\pm W^\pm jj$  background to about two orders of magnitude smaller than the DPS signal before application of further cuts. A jet veto is thus implicitly assumed in the following, and only the  $b\bar{b}$ ,  $W^\pm Z(\gamma^*)$  and  $Z(\gamma^*)Z(\gamma^*)$  backgrounds are simulated.

The basic cuts are as follows:

1. Both leptons in the like sign lepton pair must have pseudorapidity  $|\eta| < 2.5$ .
2. Both leptons are required to be isolated:  
 $E_{\text{ISO}}^l \leq E_{\text{ISO}}^{\text{min}} = 10$  GeV, where  $E_{\text{ISO}}^l$  is the hadronic transverse energy in a cone of  $R = 0.4$  surrounding each of the like-sign leptons.
3. The transverse momenta of both leptons,  $p_T^l$ , must satisfy  $20 \leq p_T^l \leq 60$  GeV.
4. An event is rejected whenever a third, opposite-signed, lepton is identified. A lepton is assumed to be identified with 100% efficiency when  $p_T^l \geq p_T^{\text{id}}$  and  $|\eta| < \eta^{\text{id}}$ , where  $p_T^{\text{id}} = 10$  GeV and  $\eta^{\text{id}} = 2.5$ .
5. The missing transverse energy  $\cancel{E}_T$  of an event must satisfy  $\cancel{E}_T \geq 20$  GeV.
6. Reject an event if a charged (lepton) track with  $p_T^{\text{id}} \geq p_T \geq 1$  GeV forms an invariant mass  $< 1$  GeV with one of the same-sign leptons.

In the above, the muons are treated as invisible particles when  $|\eta| > 2.5$ . We define  $\cancel{E}_T$  to be the magnitude of the vector  $p_T$  sum of all visible particles. Note that the above cuts are designed to be within the capabilities of the LHC general purpose detectors, ATLAS and CMS. All our cross sections are evaluated at  $\sqrt{s} = 14$  TeV.

We next discuss event simulations. The  $b\bar{b}$  events are generated using HERWIG6.510 [38]. The large total cross section  $\sigma_{b\bar{b}} \sim 500 \mu\text{b}$  means that, in practice, a parton-level cut on the transverse momentum of the bottom quarks,  $p_T^b$ , is imposed to make the simulation manageable. This parton-level cut is chosen to be  $p_T^b \geq 20$  GeV, which is motivated by one of the basic cuts,  $p_T^l \geq 20$  GeV, discussed above. The resulting lepton  $p_T$  distribution should remain unchanged, as most isolated leptons from  $B$  meson decays have  $p_T^l$  smaller than the transverse momentum of the parent  $b$  quark. To improve efficiency of event generation, we further force the  $B$  mesons to always decay semileptonically. Whenever one or more neutral  $B$  mesons are produced, exactly one of them undergoes  $B^0-\bar{B}^0$  mixing. As discussed in [39], this neglects the production of leptons in charm decays. However these leptons are expected to have a lower  $p_T$  and be less well isolated than the leptons produced in  $b$  decays. The amount of Monte Carlo data generated is equivalent to about  $200 \text{ fb}^{-1}$ . The cross section  $\sigma_{b\bar{b}}(p_T^b \geq 20 \text{ GeV})$  is then normalised to the corresponding value obtained in MCFM [40] using the central MSTW LO sPDF set. This value is found to be  $\sigma_{b\bar{b}}(p_T \geq 20 \text{ GeV}) = 5.15 \mu\text{b}$ , where the renormalisation and factorisation scales are set at  $\mu_R = \mu_F = m_b = 4.75$  GeV respectively.

Simulations of the other processes are performed at leading-order parton level only. Given that the value of  $\sigma_{\text{eff}}$ , which controls the overall magnitude of the DPS signal, is unknown at LHC energies, this approximation is

	$\sigma_{\mu^+\mu^+}$ (fb)	$\sigma_{\mu^-\mu^-}$ (fb)
$W^\pm W^\pm(\text{DPS})$	0.82	0.46
$W^\pm Z(\gamma^*)$	5.1	3.6
$Z(\gamma^*)Z(\gamma^*)$	0.84	0.67
$b\bar{b}$ ( $p_T^b \geq 20 \text{ GeV}$ )	0.43	0.43

**Table 3.** Cross sections (in fb) of the processes simulated after the basic cuts are applied, including branching ratios corresponding to same-sign dimuon production. The cross sections for  $\mu^+\mu^+$  and  $\mu^-\mu^-$  production are displayed in the second and third columns respectively. The signal cross sections are obtained assuming  $\sigma_{\text{eff}} = 14.5$  mb.

sufficient for the present purpose. The parton distributions and electroweak parameters used are discussed in Section 2. The value of  $\alpha_S(M_Z)$  is 0.13939, and we use one loop  $\alpha_S$  running throughout.

For  $W^\pm Z(\gamma^*)$  and  $Z(\gamma^*)Z(\gamma^*)$ , we obtain the matrix elements from MADGRAPH [41, 42], including both doubly and singly resonating diagrams. The phase space integration is performed using VEGAS [43]. All gauge bosons are decayed leptonically, and off-shell effects are included in the simulations. The factorisation scale is chosen to be  $\mu_F = M_W$  for all these (leading-order) processes.

The signal processes  $W^\pm W^\pm$  are generated in a similar way. Here GS09 is used, and again we set  $\mu_F = M_W$ . The effective cross section  $\sigma_{\text{eff}}$  is taken to be 14.5 mb, its value obtained by the CDF collaboration at the Tevatron. Since we use cuts on the  $p_T$  of the leptons, it is important to generate realistic  $p_T$  distributions. To account for the non-zero  $p_T$  of a  $W$  boson, we introduce a ‘ $p_T$ -smearing’. It is well known that the fixed-order perturbative calculation fails to describe the  $p_T$  distribution of single gauge bosons produced at small  $p_T$  and that the correct description is provided by the resummed calculations, supplemented by a parameterization of non-perturbative effects at very small  $p_T$ . Resummation takes into account modifications to the  $p_T$  distribution due to multiple soft gluon emission. We calculate the resummed distribution to next-to-leading logarithmic (NLL) accuracy with NLO MSTW pdfs, using the code of Ref. [44] and the non-perturbative parameterisation of Ref. [45]. The leptons originating from the two (virtual)  $W$  bosons are then boosted independently in the azimuthal plane according to the  $p_T$  distribution obtained in this way. Even though the dPDFs used in this study are leading-order quantities, which means that formally it is more consistent to adopt a leading logarithmic (LL) calculation, we argue that the described (NLL) procedure is more appropriate for our studies, since it gives a more realistic description of the  $W$   $p_T$  distribution. However it should be kept in mind that different ‘ $p_T$  smearing’ prescriptions will lead to slight changes in kinematic distributions.

The cross sections for the simulated DPS signal and background processes are displayed in Table 3. The cross sections correspond to detecting same-sign dimuon events only. Inclusion of  $e^\pm e^\pm$  and  $e^\pm \mu^\pm$  events can be estimated by multiplying the results in Table 3 by appropriate fac-



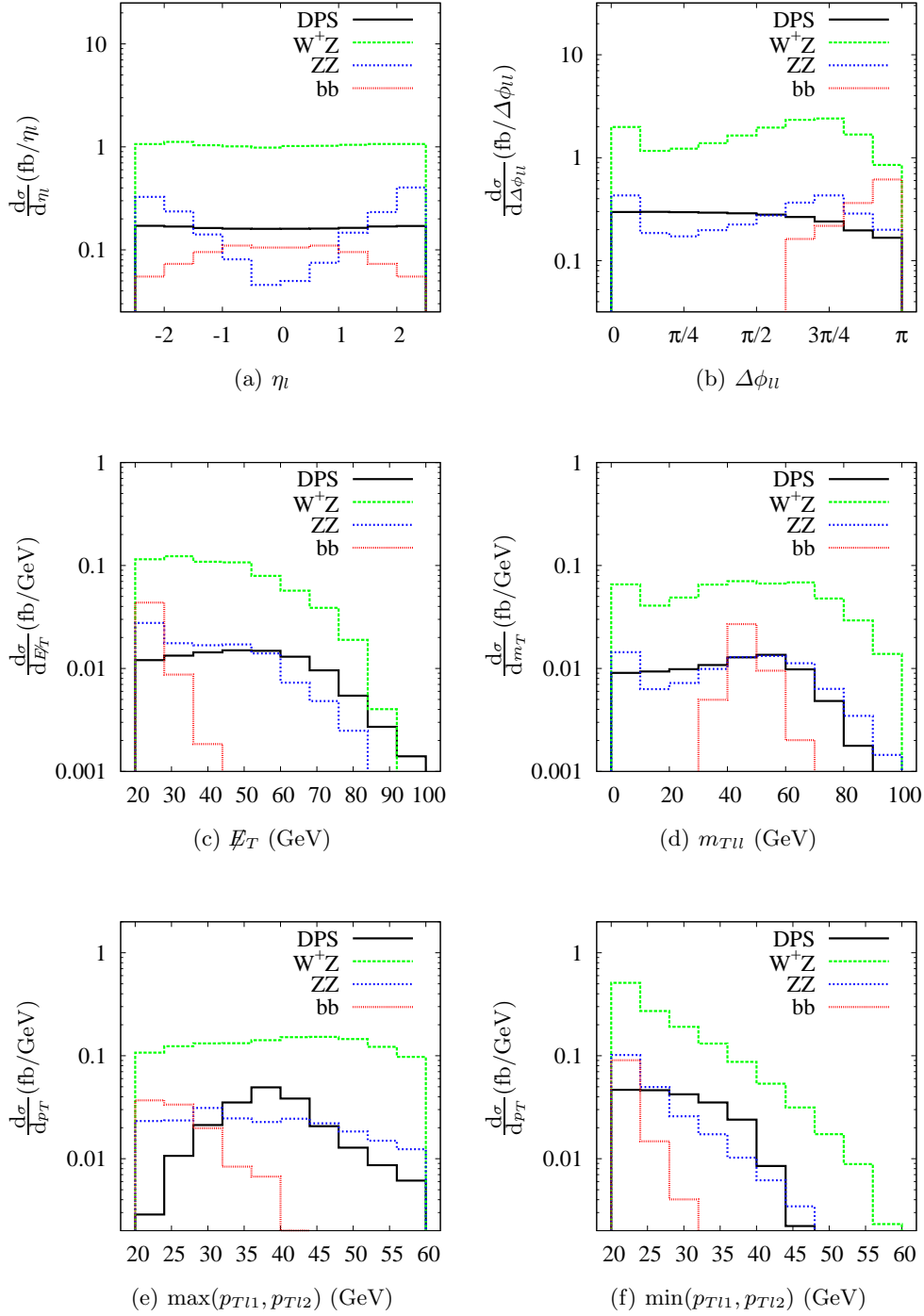


**Fig. 5.** Selected kinematic distributions for the positively charged (++) SSL events. The DPS signal,  $W^+Z(\gamma^*)$ ,  $Z(\gamma^*)Z(\gamma^*)$  and  $b\bar{b}$  backgrounds are described by solid black, green dotted, blue dotted and red dashed lines respectively.

tors.<sup>2</sup> We see that although the total  $b\bar{b}$  cross section is huge, the basic cuts are very effective in suppressing this

<sup>2</sup> Due to different dPDFs, cuts and lepton channels considered, our numerical values for the cross sections are different from those presented in Ref. [26].

background. Instead the largest background comes from  $WZ(\gamma^*)$  production, whereas the  $Z(\gamma^*)Z(\gamma^*)$  background is about a factor of 6 smaller. In the latter, we observe an asymmetry of the  $\sigma_{\mu^+\mu^+}$  and  $\sigma_{\mu^-\mu^-}$  cross sections. These two processes would have the same cross sections if the parton level amplitudes were the same upon interchange-

ing the momenta of an opposite-sign lepton pair. However this not the case, as a subset of the Feynman diagrams contributing to these processes changes sign, leading to different kinematic (in particular pseudorapidity) distributions.<sup>3</sup>

One could consider whether kinematic distributions might be able to further discriminate the signal from background. Given that the signal cross sections are only in the 1 fb region, care is required not to significantly suppress the signal.

In Fig. 5 and Fig. 6 we show some representative kinematic distributions for the positively charged ( $++$ ) and negatively charged ( $--$ ) SSL events respectively. In these figures, we use only ten bins in each plot to reflect the anticipated modest number of events expected for the femtobarn level processes considered, at least in early LHC data taking.

For the signal, the ( $++$ )  $\eta_l$  distribution is almost flat, increasing slightly towards large  $|\eta_l|$ , whereas the signal for the ( $--$ ) events shows a small central peak instead. Both of these features are characteristic of charged leptons from single Drell-Yan production. The distribution of  $\Delta\phi_{ll}$ , the angular separation of the SSL pair in the transverse plane, dips near  $\Delta\phi_{ll} = \pi$ , as the neutrinos tend to be produced back-to-back in this limit, thus reducing the missing transverse momentum  $\cancel{E}_T$ .

For the  $W^\pm Z(\gamma^*)$  contributions, small peaks appear in the  $\Delta\phi_{ll} = 0$  and  $m_{Tll} = 0$  regions. Here  $m_{Tll}$  is the transverse mass of the SSL lepton pair. These two peaks are correlated, and arise primarily from the  $\gamma^*$  contributions. The  $Z(\gamma^*)Z(\gamma^*)$  background exhibits similar peaking features for the same reason. Furthermore, the  $\eta_l$  distribution for this background peaks strongly towards the high  $|\eta|$  region. This is because the  $Z$  contributes most significantly when one of its daughter leptons is produced outside the central tracking region, pulling its partner forward as a result.

Overall, we see that while the  $b\bar{b}$  distributions are distinct from those of the signal, the dominant  $W^\pm Z(\gamma^*)$  background has kinematic distributions fairly similar to the signal. A cut on events when the lepton pair are approximately back-to-back in the transverse plane, for example  $\Delta\phi_{ll} \lesssim 0.7\pi$ , could help, but further kinematic cuts are unlikely to improve the signal to background ratio significantly. Optimisation of the cuts would in any case require a more detailed detector simulation, and is beyond the scope of this work.

On the positive side, it might be advantageous to exploit the fact that the value of  $a_{\eta_l}$  is relatively small for the DPS signal. This means that the probability of the same-sign leptons from the signal process to lie in opposite ( $\eta_1 \times \eta_2 < 0$ ) and same ( $\eta_1 \times \eta_2 > 0$ ) hemispheres are approximately equal. However for the single scattering background, the final states prefer to have small  $\Delta\eta$

in order to minimise the partonic centre-of-mass energy. This implies that  $a_{\eta_l}$  will generally be negative. In Fig. 7, we show  $a_{\eta_l}$  as a function of  $\eta_l^{\min}$  after the basic cuts are imposed. Requiring the leptons to satisfy  $\eta_{l1} \times \eta_{l2} < 0$  would reduce the signal by about a factor of 2, while reducing 2/3 of the  $W^\pm Z(\gamma^*)$  and almost all the  $Z(\gamma^*)Z(\gamma^*)$  backgrounds.

The ratio of positively charged ( $++$ ) and negatively charged ( $--$ ) SSL events may also be used. Due to the (quasi-)factorised nature of DPS production, the signal cross ratio  $\sigma_{W^+W^+}^{DPS}/\sigma_{W^-W^-}^{DPS}$  is expected to be similar to  $(\sigma_{W^+}/\sigma_{W^-})^2$ . The former ratio can be inferred from Table 2 to be about 1.8 at 14 TeV, whereas the square of  $\sigma_{W^+}/\sigma_{W^-}$  at LO is  $\sim 1.36^2 = 1.85$ . An important point is that this ratio is stable against the application of cuts, as can be inferred from the results in Table 3. Because it originates in  $gg$  scattering, the  $b\bar{b}$  background contributes equally to ( $++$ ) and ( $--$ ) lepton pair production. From Fig. 8, we see that the  $\sigma_{W^+Z}/\sigma_{W^-Z}$  ratio is roughly 1.4, a reflection of the  $u/d$  parton distribution ratio in the proton. For the  $Z(\gamma^*)Z(\gamma^*)$  process, the corresponding ratio is 1.25 after including the basic cuts.

Even though these ratios are cut dependent and would presumably change slightly after properly including higher-order effects, the presence of DPS events *predicts* that the ratio ( $++$ )/( $--$ ) would exceed the expectation from single scattering background events only.

## 5 Summary

We have studied same-sign  $W$  pair production as a potential signal of double parton scattering at 14 TeV at the LHC. We considered both the DPS signal (in the purely leptonic decay channel) and a number of backgrounds from the usual single parton scattering.

We first showed that the improved GS09 dPDFs lead to different production properties compared to naive factorisation models. In particular, the use of GS09 dPDFs leads to non-trivial rapidity correlations of the final-state leptons. Valence number conservation implies that it is unlikely to find 2 high- $x$  valence quarks of the same flavour from a single proton, resulting in a positive lepton pseudorapidity asymmetry  $a_{\eta_l}$  for the DPS processes. Otherwise, the lepton pseudorapidity distribution using GS09 can be reasonably well approximated by the MSTW<sub>1</sub> quasi-factorized model.

Our calculations of the DPS signal were undertaken with the assumption that  $\sigma_{\text{eff}}$  is a constant, and equal to the CDF measured value of 14.5 mb. We remind the reader that although this assumption is consistent with existing experimental data, it is likely that there will be a certain degree of process dependence in  $\sigma_{\text{eff}}$  [48]. It is also possible that different scale factors might be appropriate for contributions to the dPDF coming from different terms in the dDGLAP equation [31]. Unless the  $\sigma_{\text{eff}}$  for equal sign WW production at the LHC is very much smaller than the CDF value, it is likely that the theoretical aspects just described will be difficult to study in the early stages

<sup>3</sup> It is interesting to note that this happens even for diagrams involving only  $\gamma^*$  and not  $Z$ . The parton level amplitudes of these diagrams do not change under charge conjugation. However the associated PDF weights change as a result, leading to different kinematic distributions at the hadron level.

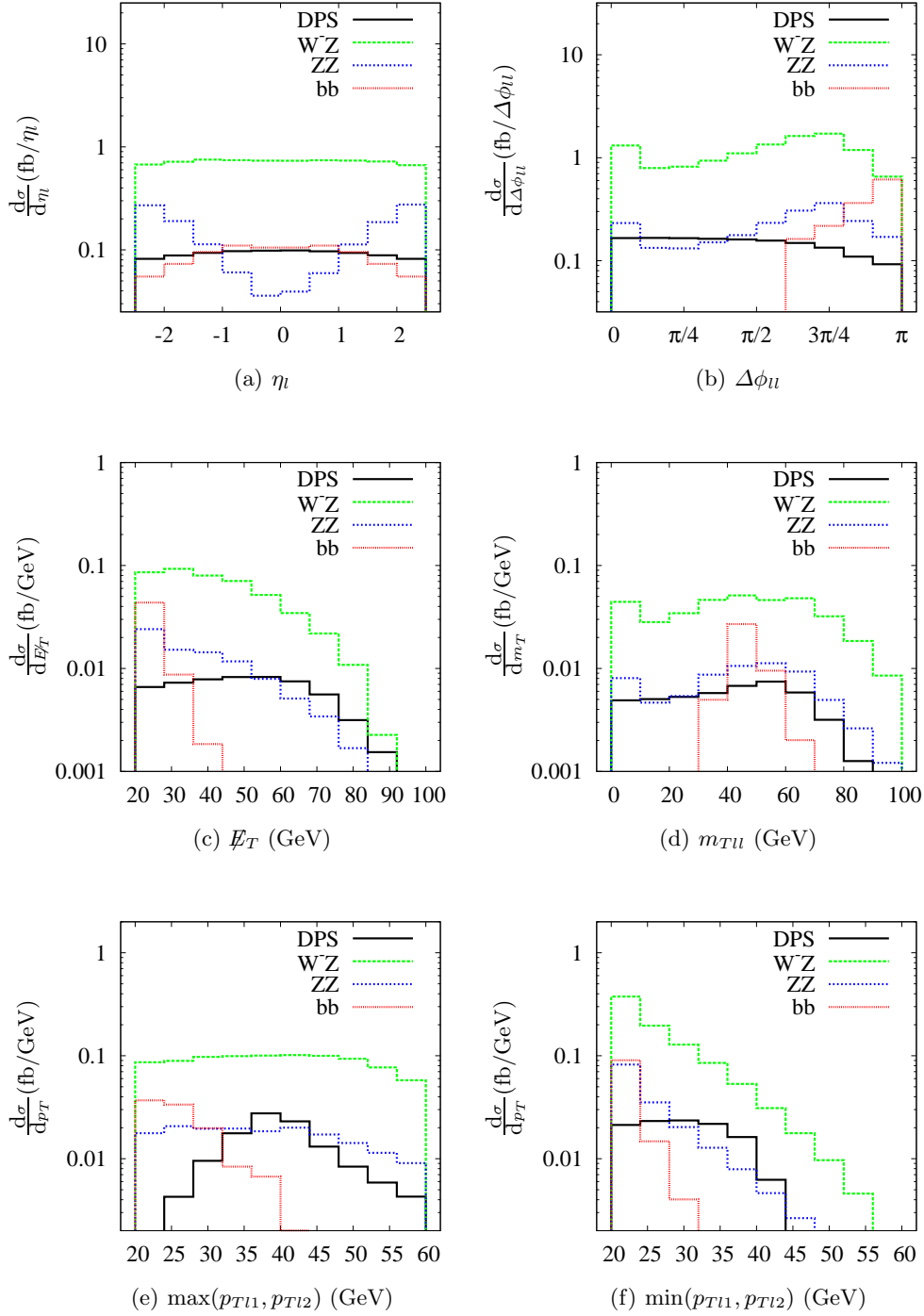


**Fig. 6.** Selected kinematic distributions for the negatively charged (—) SSL events. The DPS signal,  $W^-Z(\gamma^*)$ ,  $Z(\gamma^*)Z(\gamma^*)$  and  $b\bar{b}$  backgrounds are described by solid black, green dotted, blue dotted and red dashed lines respectively.

of LHC running due to limited statistics. However, the fundamental characteristic of the DPS signal process – two (quasi-) independent scatterings – means that  $\eta_{l1} \times \eta_{l2}$  and the  $(++)/(- -)$  event ratio could provide additional experimental handles.

On the other hand, more work needs to be done in order to suppress the background further. In addition to the  $W^\pm W^\pm jj$  background previously considered in the literature, we have also considered di-boson and heavy flavour backgrounds in some detail. Even though the ‘non-reducible’  $W^\pm W^\pm jj$  single scattering background can be

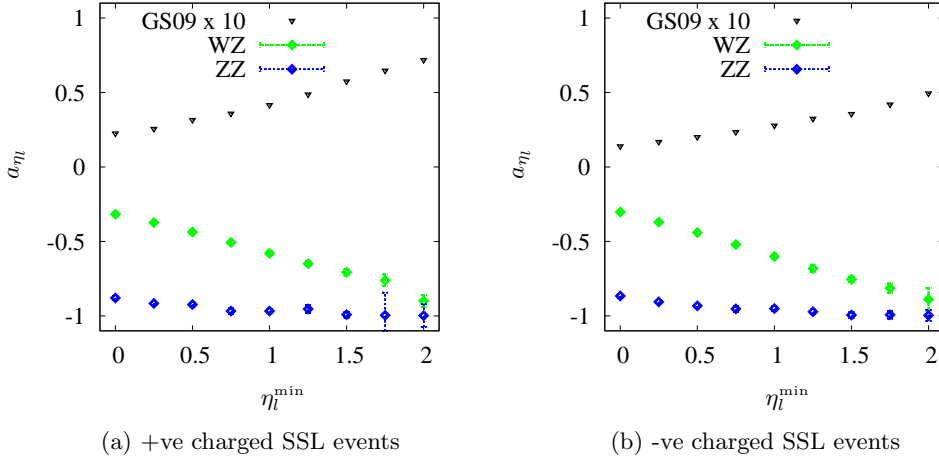


**Fig. 7.** Pseudorapidity asymmetry  $a_{\eta_l}$  as a function of  $\eta_l^{\min}$ . From top to bottom, the points correspond to the DPS signal using GS09 and the dominant backgrounds  $W^+Z(\gamma^*)$  and  $Z(\gamma^*)Z(\gamma^*)$ . For the factorised models MSTW<sub>i</sub>,  $a_{\eta_l}$  is practically zero. For clarity, the  $a_{\eta_l}$  values for the signal are multiplied by a factor of 10.

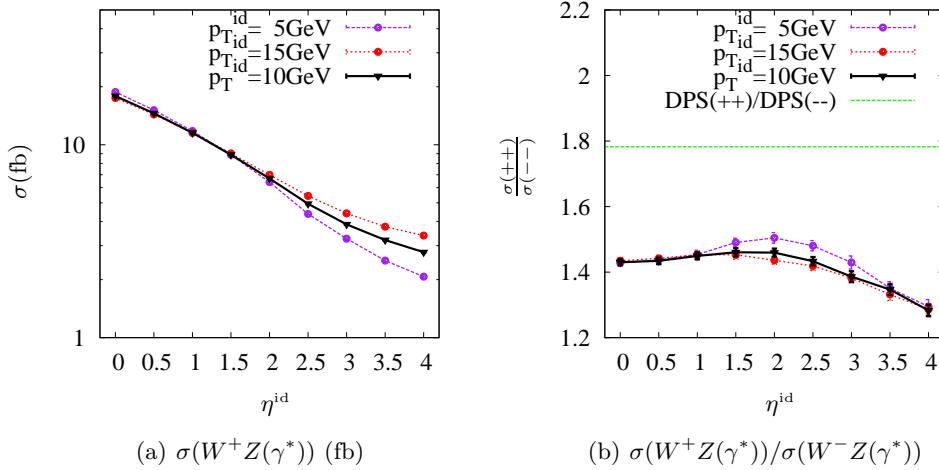


**Fig. 8.** Variation of the  $W^+Z(\gamma^*)$  cross section and the ratio  $\sigma(W^+Z(\gamma^*))/\sigma(W^-Z(\gamma^*))$  as a function of  $p_T^{\text{id}}$  and  $\eta^{\text{id}}$ . As discussed in the basic cuts in the text, the parameters  $p_T^{\text{id}}$  and  $\eta^{\text{id}}$  are the minimum  $p_T$  and maximum  $\eta$  for which a lepton can be identified. From bottom to top, the lines correspond to  $p_T^{\text{id}} = 5, 10$  and  $15$  GeV respectively. In Fig. 8(b), the ratio for the DPS signal is also shown.

effectively suppressed by a central jet veto, the di-boson background remains significant after applying a fairly basic set of cuts. Using the canonical  $\sigma_{\text{eff}} = 14.5$  mb to calibrate the DPS signal, we find that the diboson background can be a factor of a few larger than the signal.

Given the exploratory nature of this study, we have not included either detector effects or higher-order perturbative corrections. Given the similarity between the  $W^\pm Z(\gamma^*)$  and signal distributions, it might not be very beneficial to impose simple additional physics cuts. However, the Standard Model processes leading to tri-lepton events will be studied in detail at the LHC. An in-depth

understanding of this process might allow accurate extrapolation into our region of interest, where one of the leptons is not detected. This would provide an important calibration of the diboson background. Furthermore, ‘detector cuts’ could also be made. For example, tighter lepton isolation and wrong-sign lepton vetos could be used. Extending the pseudorapidity region where a (wrong sign) lepton can be identified could also be useful. Displaced charged lepton vertices might also be helpful in further reducing the  $b\bar{b}$  background.

In summary, our preliminary ‘first look’ analysis has shown that a small excess of SSL events from double par-

ton scattering could be observed at the LHC, and we are optimistic that further improvements can be made to enhance the signal.

**Acknowledgements** We are grateful to Richard Batley for helpful discussions. A.K. would like to thank the HEP Group at the Cavendish Laboratory for warm hospitality and A. Mück for useful discussions. J.G. acknowledges financial support from the UK Science and Technology Facilities Council.

## Appendix: multiple particle interaction

Given a luminosity ( $L$ ), a single scattering cross section ( $\sigma$ ) and rate of bunch crossing ( $B$ ), the average number of events per bunch crossing,  $\langle n \rangle$ , is given by

$$\langle n \rangle = \frac{L\sigma}{B}. \quad (11)$$

Using Poisson's statistics, this can be translated into a multiple particle interaction cross section,  $\sigma_N$ , where

$$\begin{aligned} \sigma_N &= e^{-\langle n \rangle} \frac{\langle n \rangle^N}{N!} \frac{B}{L} \\ &\simeq \frac{\sigma^N}{N!} \left( \frac{L}{B} \right)^{N-1}, \end{aligned} \quad (12)$$

where the last equation holds if  $\langle n \rangle \ll 1$ . An effective multiple particle interaction parameter,  $\sigma_{N,\text{eff}}$ , can be defined analogous to  $\sigma_{\text{eff}}$  for multi-parton interaction:

$$\begin{aligned} \sigma_N &= \frac{\sigma^N}{N!(\sigma_{N,\text{eff}})^{N-1}}, \\ \sigma_{N,\text{eff}} &\equiv \left( \frac{B}{L} \right). \end{aligned} \quad (13)$$

The above approximation ceases to be valid when  $\sigma \sim \sigma_{N,\text{eff}}$ , which implies also that  $\langle n \rangle \sim 1$ . For  $B = 4 \cdot 10^7 \text{ s}^{-1}$  and  $L = 10^{34} \text{ cm}^{-2} \text{ s}^{-1}$ , we get  $\sigma_{N,\text{eff}} = 4 \text{ mb}$ . However, in double particle interactions, the two interaction vertices typically do not overlap. Using the RMS bunch length of 7.5 cm [46] and intrinsic z-resolution of 115  $\mu\text{m}$  and 580  $\mu\text{m}$  for the Pixel detector and SCT at ATLAS [47] respectively, the probability that 2 independent scatterings overlap each other is estimated to be of the order  $\mathcal{O}(0.1)\%$ . As a result this background contribution to double parton scattering, assuming  $\sigma_{\text{eff}} = 14.5 \text{ mb}$ , can be safely neglected.

## References

1. P. V. Landshoff and J. C. Polkinghorne, Phys. Rev. D **18** (1978) 3344.
2. F. Takagi, Phys. Rev. Lett. **43** (1979) 1296.
3. C. Goebel, F. Halzen and D. M. Scott, Phys. Rev. D **22** (1980) 2789.
4. N. Paver and D. Treleani, Nuovo Cim. A **70** (1982) 215.
5. B. Humpert, Phys. Lett. B **131** (1983) 461.
6. M. Mekhfi, Phys. Rev. D **32** (1985) 2371.
7. B. Humpert and R. Odorico, Phys. Lett. B **154** (1985) 211.
8. L. Ametller, N. Paver and D. Treleani, Phys. Lett. B **169** (1986) 289.
9. M. Mekhfi, Phys. Rev. D **32** (1985) 2380.
10. F. Halzen, P. Hoyer and W. J. Stirling, Phys. Lett. B **188** (1987) 375.
11. T. Sjostrand and M. van Zijl, Phys. Rev. D **36** (1987) 2019.
12. M. L. Mangano, Z. Phys. C **42** (1989) 331.
13. R. M. Godbole, S. Gupta and J. Lindfors, Z. Phys. C **47** (1990) 69.
14. M. Drees and T. Han, Phys. Rev. Lett. **77** (1996) 4142 [arXiv:hep-ph/9605430].
15. G. Calucci and D. Treleani, Nucl. Phys. Proc. Suppl. **71** (1999) 392 [arXiv:hep-ph/9711225].
16. G. Calucci and D. Treleani, Phys. Rev. D **60** (1999) 054023 [arXiv:hep-ph/9902479].
17. T. Akesson *et al.* [Axial Field Spectrometer Collaboration], Z. Phys. C **34** (1987) 163.
18. F. Abe *et al.* [CDF Collaboration], Phys. Rev. D **56** (1997) 3811.
19. V. M. Abazov *et al.* [D0 Collaboration], Phys. Rev. D **81** (2010) 052012 [arXiv:0912.5104 [hep-ex]].
20. A. Del Fabbro and D. Treleani, Phys. Rev. D **61** (2000) 077502 [arXiv:hep-ph/9911358].
21. A. Del Fabbro and D. Treleani, Phys. Rev. D **66** (2002) 074012 [arXiv:hep-ph/0207311].
22. M. Y. Hussein, Nucl. Phys. Proc. Suppl. **174** (2007) 55 [arXiv:hep-ph/0610207].
23. M. Y. Hussein, arXiv:0710.0203 [hep-ph].
24. A. Kulesza and W. J. Stirling, Phys. Lett. B **475** (2000) 168 [arXiv:hep-ph/9912232].
25. E. Maina, JHEP **0904** (2009) 098 [arXiv:0904.2682 [hep-ph]].
26. E. Maina, JHEP **0909** (2009) 081 [arXiv:0909.1586 [hep-ph]].
27. E. L. Berger, C. B. Jackson and G. Shaughnessy, Phys. Rev. D **81** (2010) 014014 [arXiv:0911.5348 [hep-ph]].
28. A. M. Snigirev, Phys. Rev. D **68** (2003) 114012 [arXiv:hep-ph/0304172].
29. J. R. Gaunt and W. J. Stirling, JHEP **1003** (2010) 005 [arXiv:0910.4347 [hep-ph]].
30. V. L. Korotkikh and A. M. Snigirev, Phys. Lett. B **594** (2004) 171 [arXiv:hep-ph/0404155].
31. E. Cattaruzza, A. Del Fabbro and D. Treleani, Phys. Rev. D **72** (2005) 034022 [arXiv:hep-ph/0507052].
32. D. Treleani, slides presented at MPI at LHC workshop, 27-31 Oct 2008, Perugia, Italy, <http://agenda.infn.it/getFile.py/access?contribId=8&sessionId=2&resId=0&materialId=slides&confId=599>
33. P. Bartalini *et al.*, arXiv:1003.4220 [hep-ex].
34. A. Novoselov, slides presented at Physics and Computing in ATLAS meeting, 16-19 Sept 2008, IHEP, Protvino, <http://pcbec3.ihep.su/~miagkov/meet08-2/pr-novoselov-gamma.pdf>
35. Z. Sullivan and E. L. Berger, Phys. Rev. D **74** (2006) 033008 [arXiv:hep-ph/0606271].
36. C. Amsler *et al.* [Particle Data Group], Phys. Lett. B **667** (2008) 1.
37. M. S. Chanowitz and W. B. Kilgore, Phys. Lett. B **347** (1995) 387 [arXiv:hep-ph/9412275].
38. G. Corcella *et al.*, JHEP **0101** (2001) 010 [arXiv:hep-ph/0011363].

- 39. H. K. Dreiner, P. Richardson and M. H. Seymour, Phys. Rev. D **63** (2001) 055008 [arXiv:hep-ph/0007228].
- 40. J. M. Campbell and R. K. Ellis, <http://mcfm.fnal.gov/>.
- 41. F. Maltoni and T. Stelzer, JHEP **0302** (2003) 027 [arXiv:hep-ph/0208156].
- 42. T. Stelzer and W. F. Long, Comput. Phys. Commun. **81** (1994) 357 [arXiv:hep-ph/9401258].
- 43. G. P. Lepage, J. Comput. Phys. **27** (1978) 192.
- 44. A. Kulesza and W. J. Stirling, Nucl. Phys. B **555** (1999) 279 [arXiv:hep-ph/9902234];  
A. Kulesza and W. J. Stirling, Eur. Phys. J. C **20** (2001) 349 [arXiv:hep-ph/0103089].
- 45. A. Kulesza and W. J. Stirling, JHEP **0312** (2003) 056 [arXiv:hep-ph/0307208].
- 46. F. Zimmermann, slides presented at LARP Mini-Workshop On Beam-Beam Compensation, 2-4 Jul 2007, Menlo Park, California, <http://www.slac.stanford.edu/spires/find/hep/www?irn=7494106>.
- 47. G. Aad *et al.* [The ATLAS Collaboration], arXiv:0901.0512 [hep-ex].
- 48. A. Del Fabbro and D. Treleani, Phys. Rev. D **63**, 057901 (2001) [arXiv:hep-ph/0005273].

